

# Automated Land Cover Mapping Using Landsat Thematic Mapper Images and Topographic Attributes

Jonathan M. Wheatley, John P. Wilson, Roland L. Redmond, Zhenkui Ma, and Jeff DiBenedetto

## 15.1 INTRODUCTION

Land managers must know the geographical distribution of landscape components such as vegetation, soils, and terrain to manage natural resources effectively. The need for natural resource mapping has long been acknowledged:

A vegetation map not only serves as a record of what exists when it is made, but also as a starting point for the study of changes, whether natural or brought about by human activity. It serves to arouse public interest of a country in its wild vegetation, which ought to be recognized as a national possession not to be lightly destroyed or wasted, and it indicates the localities which are most suitable for the nature reserves which every country should have. The making of such maps should be part of the national stock-taking which is the duty of every modern community (Tansley and Chipp 1926).

The production of detailed resource maps was costly, time-consuming, and not easily standardized before the advent of digital remote sensing and computerized image analysis. Such maps were compiled from decades of fieldwork that could not be updated quickly. Geographic information systems (GIS) and remote sensing now provide tools for mapping large areas at spatial resolutions as fine as 30 m, and potentially allow these maps to be updated efficiently (Tueller 1989, Franklin 1995, Gerrard et al. 1997).

*Landsat* multispectral remote sensing attempts to identify vegetation based on its spectral reflectance, measured in the satellite's seven wavelength bands, ranging

from blue visible light to far-infrared thermal wavelengths (Niemann 1993). Generally, green leaves absorb light in the 0.4- to 0.7- $\mu\text{m}$  wavelength range, but make an abrupt transition to reflectance at 0.7  $\mu\text{m}$ , scattering light effectively between 0.7 and 1.3  $\mu\text{m}$  (Gates et al. 1965, Ripple 1985). In the semiarid grassland and badland cover types that are common in the Little Missouri National Grassland (LMNG) of western North Dakota, the observed reflectance may result from a combination of live vegetation, dead vegetation, and bare soil. In addition, the spectral signature may vary due to differing angles of illumination, the health of vegetation (affected by precipitation and grazing), and the seasonal life cycle of vegetation (Tueller 1989). The ability of *Landsat* Thematic Mapper (TM) to distinguish vegetation types is often limited by the spectral and spatial resolution of the detector (Niemann 1993).

Two general types of classification are used: unsupervised and supervised. In the former, the data are clustered into arbitrary categories, but in the latter, ground-truth is used as training data to divide the multidimensional data space into categories based on the observed properties of the training data set (Jensen 1996). Provided that adequate, unbiased training data are available, supervised methods are far superior to the arbitrary classes generated with unsupervised methods.

Numerous statistical clustering methods have been used to group multispectral data into land cover classes, but ultimately, the quantity and quality of ground-truth data used for the supervised classification of vegetation classes may be more important than the classification method used (Congalton 1991). In one such study, Zhuang et al. (1995) compared minimum distance, maximum likelihood, and neural network classification accuracy for six land cover classes in a mixed cropland, rangeland, and broadleaf forest site in Indiana. The three methods produced similar accuracies ( $\pm 5\%$ ) for each of the land cover classes, with the exception of the bare soil class, where the neural network classifier was 10% more accurate than the other two methods. As with many remote sensing applications, accuracies of 85–95% could be achieved only by lumping land cover types into very broad categories: water, bare soil, one forest class, one grassland class, and two crop classes (Zhuang et al. 1995).

Most automated remote sensing classification methods are not able to distinguish ecologically distinct vegetation types of interest to the land manager. Anderson et al. (1976) defined a hierarchy of land cover types: Land managers are typically interested in Anderson level III vegetation categories (the species level), but automated classification accuracies for these classes are generally quite low,  $\leq 65\text{--}75\%$  (Skidmore and Turner 1988). This result occurs because there is no simple correlation between vegetation type and spectral signature. Considerable confusion arises because dissimilar vegetation types may have similar spectral signatures. Furthermore, a given vegetation type may have a seasonally variable signature. Grasslands, in particular, show rapid responses to varying precipitation amounts (Pickup et al. 1994). Regardless of future improvements in remote sensing technology, such as imaging spectrometers, which produce a reflectance spectrum for each pixel in the image, there will always be some inherent confusion between spectral reflectance and land cover (Wilkinson 1996).

An alternative approach to identifying vegetation by species is to characterize it by ecological parameters, such as leaf area index (LAI) or above-ground biomass,

that are less arbitrarily related to the plant's spectral reflectance than genus and species (Anderson et al. 1993, Paruelo and Lauenroth 1995). However, establishing a universal relationship between remote sensing spectral indices, such as the Normalized Difference Vegetation Index (NDVI), and ecological parameters has sometimes proved difficult. In Great Plains grasslands at Mandan, ND, Aase et al. (1987) found that the relationship between NDVI and LAI varied according to the intensity of cattle grazing, making it impossible to translate NDVI into LAI without knowing the grazing intensity. Friedl et al. (1995) reported similar problems in the Konza Prairie, KS. The rapid temporal variation of the spectral signature and interplay of forces, such as drought and grazing, would seem to provide special challenges for those interested in automated mapping of rangeland cover types over large areas.

Topographic attributes are increasingly utilized in remote sensing classifications. In one such study, Niemann (1993) used three topographic attributes (elevation, slope gradient, aspect) and location (an easting to measure distance along a gradient between the interior and coastal biogeoclimatological zones) with *Landsat* TM information to identify eight conifer classes in the old-growth forest of southwestern British Columbia. Only three of the eight classes (which varied in terms of species composition, age class, and crown closure) yielded accuracy results > 50%. The low overall accuracy (~45%) was attributed to two factors: (1) Different conifer stands displayed similar spectral reflectances, and (2) many of the age differences were related to past land use practices or disturbance history that was not well correlated with site characteristics. In another study, Joria and Jorgenson (1996) used ancillary data layers of elevation, slope, landform type, solar radiation, and riparian zones in a postclassification rule-based model to classify 14 arctic tundra cover types. Classification accuracy remained at ~50% when these topographic attributes were used. One potential advantage of the statistical clustering method used in the first application is that it does not involve assumptions about the relationship between vegetation and terrain, whereas rule-based classifiers may involve subjective rules and broad assumptions about terrain-vegetation correlations. Often, rule-based classifiers are specific to a particular area, whereas general statistical clustering is less site-dependent.

We explored whether topographic attributes could be used to improve the accuracy of remote sensing land cover maps in the LMNG. We compared the accuracy of vegetation maps prepared with an existing remote sensing classification method and varying numbers of topographic attributes to determine whether application of these methods is worthwhile over the entire Little Missouri region. Topographic attributes were examined because topographic data were available (unlike soil and climate data) at an appropriate scale in this study area. Modern soil surveys are available for less than 50% of the study area, and where 1:24,000 scale soil maps are available, they do not resolve individual wooded valleys and small drainages, but lump together much of the highly dissected badlands as "mixed badlands complex" (Aziz 1989). The climate of western North Dakota does not exhibit the dramatic elevation-induced variations seen in more mountainous terrain: The climate within the study area is quite homogenous (Owenby and Ezell 1992) and is therefore of little use in differentiating vegetation types. We were particularly interested in two vegetation-related

parameters that may be improvements over the basic parameters of elevation, slope, and aspect: (1) the spatial pattern of soil moisture as affected by slope and upslope contributing area, and (2) solar radiation as affected by topographic shading from nearby features. Both indices mimic physical processes not addressed by slope and aspect alone. Thus, one might expect these secondary topographic attributes to correlate with vegetation better than slope and aspect. We also examined the sensitivity of predicted land cover maps to the level of spatial aggregation and types of source data that were utilized.

## 15.2 DESCRIPTION OF STUDY AREA

Our study area was a 1700-km<sup>2</sup> portion of the LMNG (Figure 15.1) delineated by five 7.5' USGS quadrangles (i.e., the Tracy Mountain, Cliffs Plateau, Deep Creek North, Spring Creek, and Juniper Spur quads). This area was selected for four reasons. First, it has relatively high vertical relief (farther east the terrain is very flat, the USGS digital data errors become more troublesome, and the effects of terrain on vegetation are less dramatic). Second, these five quadrangles contained the highest density of ground-truth data. Third, the area included all the major landscape types of the Little Missouri (i.e., rolling uplands, wooded draws, badlands, river floodplains, and terraces). Fourth, they contained the Third Creek catchment that drains into the Little Missouri River and we needed to be able to delineate upslope contributing areas to calculate the topographic wetness index.

The erosional processes that created the North Dakota badlands began more than 600,000 years ago, when the continental ice sheet displaced the Little Missouri River southward into a shorter, steeper channel. The Little Missouri and its tributaries continue to cut into the surrounding plain. The eastern boundary of this erosion bisects the study area, dividing it into two dramatically different physiographic regions: the gently rolling Missouri Slope Upland to the east and the Little Missouri Badlands to the west (Bluemle 1975).

The bedrock is entirely sedimentary, consisting of Upper Cretaceous and Tertiary shale strata. The Bullion Creek Formation, which underlies most of the study area, consists of alternating layers of sandstone, shale, and lignite. Flat-topped buttes (monadnocks) of the more resistant sandstone rise 150 m above the surrounding penplain. Total vertical relief in the study area is less than 250 m. The Little Missouri has incised a channel 100–200 m below the surrounding terrain. Most of the wooded draws have V-shaped cross sections, but the larger channels have floodplains that are several hundred meters wide, and the Little Missouri River itself has a floodplain up to one kilometer wide. Pleistocene river terraces, containing material eroded from the Rocky Mountains, cover areas up to 10 km<sup>2</sup> near the main channel of the Little Missouri River. A distinctive feature of this area is the presence of naturally fired clay (clinker, locally named "scoria"), which is more erosion resistant than unbaked materials and forms steep-sided knobs 20–40 m high (Bluemle 1975). In places these knobs, together with depressions caused by the collapse of burned lignite beds, form large areas of hummocky terrain. This highly complex terrain is

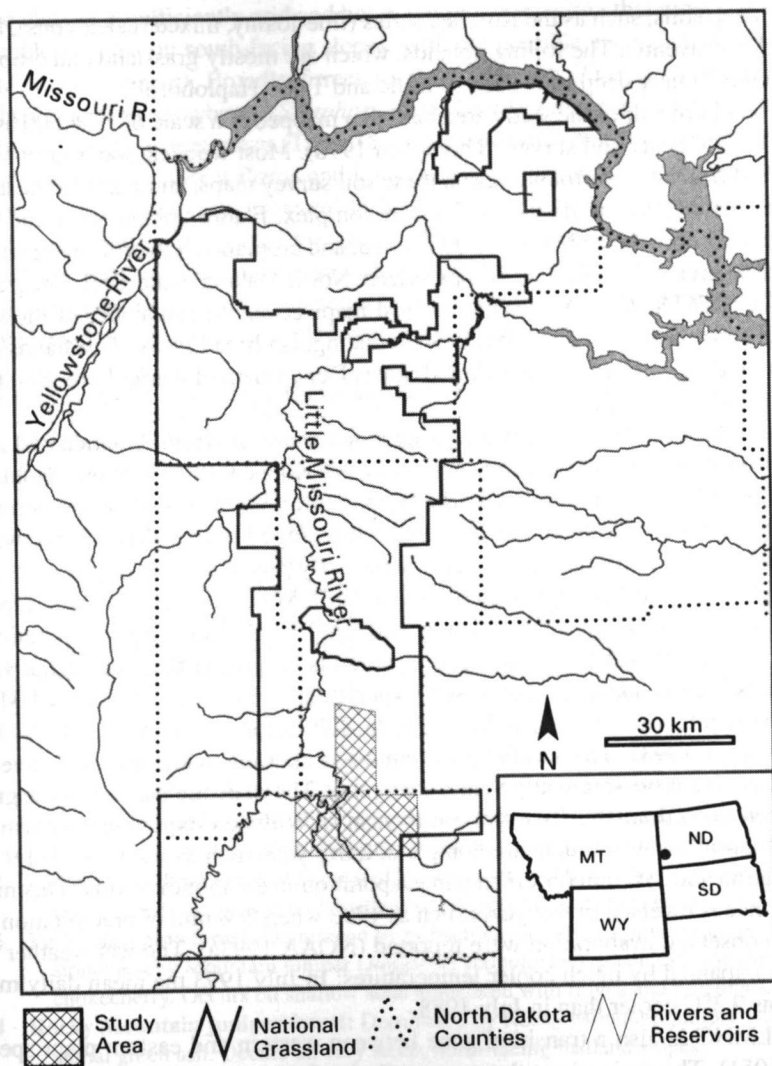


Figure 15.1. Study area map.

barely resolved at the 30-m cell size of the *Landsat* TM images and USGS digital elevation models (DEMs).

Soil is largely absent in the badlands because the steep slopes are continually eroding. Where the parent materials are sufficiently weathered to be considered soil, Inceptisols and Entisols are common, such as the Cherry (fine-silty, mixed, frigid Typic Ustochrepts) and Cabbart (loamy, mixed (calcareous), frigid, shallow Ustic Torriorthents) series, two of the more common soils in the wooded draws (Thompson 1978). The floodplains of the larger creeks are also classified as Entisols, though they

may be deep soils, such as the Korchea series (fine-loamy, mixed (calcareous), frigid Mollic Ustifluvents). The rolling uplands, which are mostly grassland and cropland, contain moderately deep soils such as Entic and Typic Haploborolls.

The southern half of the study area has been mapped at a scale of 1:24,000 as part of the Slope County soil survey (Thompson 1978). Most wooded draws are not distinguished from their surroundings on these soil survey maps, and many of these features are mapped as the Badlands-Cabbart complex. Flatter upland areas and wide floodplains within the badlands are delineated, and cropland on the rolling uplands is mapped at greater detail. The computerized North Dakota State Soil Geographic Database (STATSGO, 1:250,000 scale) soil maps cover the remainder of the study area and show even less detail, but they do distinguish broad areas of badlands from the surrounding rolling uplands (United States Department of Agriculture-Soil Conservation Service 1993).

North Dakota is located near the geographic center of North America and has a semiarid midlatitude steppe climate (BSk in the Köppen classification). Cold, dry winters ( $-15^{\circ}\text{C}$  mean monthly average temperature) alternate with warm summers ( $21^{\circ}\text{C}$  mean monthly average temperature) that average 120 frost-free days (Owenby and Ezell 1992). Precipitation is greatest in the early part of the growing season: 50% of the 400 mm annual precipitation occurs in April, May, and June, compared to <30 mm in the three winter months (Owenby and Ezell 1992). The temporal variation of precipitation from year to year at a given station is far greater than the spatial variation across North Dakota. At Dickinson Experimental Farm, just east of the LMNG, annual precipitation has ranged from 170 to 800 mm over the period 1904-1993 (Hydrosphere 1993). The rainfall distribution is skewed, with drier than average years occurring more frequently than wetter years. The moisture balance in the growing season shifts dramatically from year to year. At Williston Experimental Farm, the nearest station for which data are complete, a dry year such as 1988 yielded 9 mm precipitation and 290 mm observed pan evaporation in the month of July. This moisture balance is reversed in wet years such as 1993 when 208 mm of precipitation and 136 mm observed evaporation were reported (NOAA 1993a). The wet weather was also accompanied by much cooler temperatures: In July 1993 the mean daily maximum was  $9.3^{\circ}\text{C}$  cooler than in July 1988.

The LMNG is also a transition zone between western and eastern plant species (Rudd 1951). The region is at the western limit of the range of eastern hardwoods, such as green ash (*Fraxinus pennsylvanica*) and bur oak (*Quercus macrocarpa*), and at the eastern limit of western species, such as Rocky Mountain juniper (*Juniperus scopulorum*) and ponderosa Pine (*Pinus ponderosa*) (Little 1971). Furthermore, the area is the southernmost extent of some boreal forest trees, such as balsam poplar (*Populus balsamifera*) and paper birch (*Betula papyrifera*). Desert plants with ranges centered on the Great Basin, such as cactus (*Opuntia fragilis*), yucca (*Yucca glauca*), saltbush (*Atriplex* sp.), skunkbrush (*Sarcobatus vermiculatus*), saltgrass (*Distichlis stricta*), and sagebrush (*Artemisia tridentata*) are also widespread in the Little Missouri region (Rudd 1951). However, they may not grow in patches large enough to be detected by remote sensing.

The climate is sufficiently arid and hot in the growing season that most tree species are unable to grow on south-facing slopes, with the possible exception of ponderosa pine (*Pinus ponderosa*). Broadleaf trees such as green ash (*Fraxinus pennsylvanica*) and shrubs such as snowberry (*Symphoricarpos occidentalis*) are largely confined to woody draws near watercourses (Table 15.1). Brown (1993) mapped species composition of grasses in the Great Plains and found western wheatgrass (*Agropyron smithii*) and needle-and-thread (*Stipa comata*) to be the most common "cool-season" grasses (C3 photosynthesis path), and blue grama (*Bouteloua gracilis*) is the only "warm-season" (C4 photosynthesis path) grass in western North Dakota. Crested wheatgrass (*Agropyron desertorum*), an introduced bunchgrass from the Russian steppe, was abundantly planted to prevent erosion on former croplands abandoned during the Dust Bowl.

**TABLE 15.1 Land Cover Type Codes and Descriptions (as delineated by DiBenedetto)**

<b>2100</b>	<b>Cropland, cultivated pasture, and hay</b>
<b>3110</b>	<b>Low grass/low cover:</b> Blue grama ( <i>Bouteloua gracilis</i> ), needle-and-thread ( <i>Stipa comata</i> ), and threadleaf sedge ( <i>Carex filifolia</i> ) with low biomass productivity (less than 800 kg/ha), low ground cover, and extensive bare ground. Occurs on ridgetops and clay outwash areas below buttes.
<b>3111</b>	<b>Low grass/moderate cover:</b> Needle-and-thread, western wheatgrass ( <i>Agropyron smithii</i> ), and blue grama with medium biomass productivity, moderate ground cover, and less bare ground than cover class 3110. Typically occurs on hillslopes.
<b>3201</b>	<b>Mesic upland shrub:</b> Snowberry ( <i>Symphoricarpos occidentalis</i> ), buffaloberry ( <i>Shepherdia argentea</i> ), chokecherry ( <i>Prunus virginiana</i> ), and creeping juniper ( <i>Juniperus horizontalis</i> ) with occasional young green ash ( <i>Fraxinus pennsylvanica</i> ) trees. Occurs on north-facing slopes and in depressions and draws.
<b>3309</b>	<b>Sagebrush:</b> Silver sagebrush ( <i>Artemisia americana</i> ) with snowberry as a co-dominant shrub in some locations and a western wheatgrass/blue grama understory. Occurs mainly in valley bottoms and on terraces adjacent to stream channels.
<b>4102</b>	<b>Upland broadleaf forest:</b> Dominated by green ash and found mostly on steep, north-facing slopes associated with badlands or deeply incised channels and draws.
<b>4206</b>	<b>Ponderosa pine forest:</b> Dominated by ponderosa pine ( <i>Pinus ponderosa</i> ) with occasional Rocky Mountain juniper ( <i>Juniperus scopulorum</i> ), green ash, snowberry, and chokecherry. Occurs on shallow soils associated with ridges and hillslopes.
<b>4214</b>	<b>Rocky Mountain juniper forest:</b> Dominated by Rocky Mountain juniper with occasional green ash. Occurs on very steep, north-facing badland slopes.
<b>5000</b>	<b>Water</b>
<b>6102</b>	<b>Riparian broadleaf forest:</b> Dominated by green ash. Occurs along river bottoms and narrow draws.
<b>6201</b>	<b>Riparian grass and forb:</b> Western wheatgrass, baltic rush ( <i>Juncus balticus</i> ), and a mixture of forbs. Occurs along channel bottoms and draws.
<b>6202</b>	<b>Riparian shrub:</b> Snowberry, buffaloberry, and chokecherry with occasional young ash trees. Occurs in channel bottoms, valley bottoms, and narrow draws.
<b>7601</b>	<b>Badland:</b> Scattered patches of grass and big sagebrush ( <i>Artemisia tridentata wyomingensis</i> ) shadscale ( <i>Atriplex confertifolia</i> ), green rabbitbrush ( <i>Chrysothamnus visidiflorus</i> ), and greasewood ( <i>Sarcobatus vermiculatus</i> ). Occurs on steep, south-facing badland slopes and in outwash areas at the base of buttes and slopes.

## 15.3 METHODS AND DATA SOURCES

### 15.3.1 *Landsat*TM Image Classification

A cloud-free *Landsat* Thematic Mapper image (path 34, row 28) dated 5 July 1989 was used because no more recent cloud-free images were available for the growing season at the start of this study. This image was terrain-corrected and georeferenced to an Albers conical equal area projection by Hughes STX Corporation. We did not evaluate the spatial accuracy of this terrain correction, but it appeared to register very well with the other digital data for the area, including roads and streams from U. S. Forest Service 1:24,000 scale cartographic feature files.

Land cover was classified using a multistep method developed for mapping large (10,000–100,000 km<sup>2</sup>) areas (Ma and Redmond 1993, Ma et al. 2000). The first step used bands 3, 4, and 5 for each 30-m *Landsat* TM pixel and applied an unsupervised clustering algorithm, which is closely related to the widely used color-quantization scheme for approximating three-color composite images in a single 8-bit color image (Heckert 1982, Ma et al. 2000). The resulting vegetation classes were color-coded to resemble their appearance in a red–green–blue (RGB) color composite of the three bands, allowing easy visual inspection of the classification, and comparisons with the original image.

Image pixels were spatially grouped into three ecologically relevant patch sizes to eliminate the visual confusion of “salt-and-pepper” pixels during the second step. Three minimum map unit thresholds of 0.36 ha (5 cells), 0.81 ha (9 cells), and 2.0 ha (23 cells) were used to evaluate the trade-offs between map clarity and detail. Care must be taken to avoid removing ecologically important features such as woody draws and riparian corridors, which are prevalent in the LMNG. Vegetation classes that did not occur in patches as large as these minimum map units were eliminated, resulting in fewer classes in the aggregated image. An additional advantage of aggregation is that it greatly speeds subsequent computation and reduces data storage requirements because later classifications are performed on the raster polygons rather than individual image pixels (Ma and Redmond 1996). The remaining four *Landsat* TM bands (1, 2, 6, and 7) and selected topographic attributes were then averaged within each raster polygon to obtain mean attribute values for each patch.

The third step consists of a supervised nonparametric classification that assigns a cover type label to each patch based on the nearest distance in multidimensional parameter space to one of the ground reference “training” plots. In this study, 9, 10, or 11 data layers were used, depending on how many topographic attributes were included in the classification. The advantage of this “nearest member of group” classification is that it does not depend on any assumptions about the statistical distribution of parameters. Several cumulative topographic attributes, such as upslope contributing area and the two topographic wetness indices, were not normally distributed.

A fourth, optional step provides a postclassification sorting of riparian and upland land cover classes with similar spectral signatures using a stream buffer defined by an elevation threshold. The stream channels can be input either from USGS digital line

graph (DLG) hydrography data or from drainage channels computed by terrain analysis software such as TAPES-G, and the buffer is calculated with the same DEM data used to calculate other topographic attributes (see below). The supervised, nonparametric classification (third step) is repeated using a smaller minimum map unit inside the riparian buffer in some applications. In this study, we used an elevation difference of 5 m to define the width of the riparian zone and we examined whether the reclassification of land cover types to the appropriate riparian or upland designation (based on their occurrence inside or outside this zone) improved overall performance.

### 15.3.2 Digital Elevation Models

The five USGS 7.5' 30-m DEMs (Figure 15.1) were joined and reprojected in ARC/INFO from the original Universal Transverse Mercator (UTM) projection to the same Albers projection as the *Landsat* TM image. The digital elevation data conformed to USGS map accuracy level one that allows a mean elevation error of 7 m in a 7.5' quadrangle (United States Geological Survey 1993). However, the systematic and spatially patterned nature of the error can sometimes be confused with real terrain features in an area such as the LMNG where the total vertical relief is as little as 20 m in some quadrangles. Several examples of the types of error that can occur in USGS elevation data are illustrated in Figure 15.2, which shows a 16 × 22-km area located at the southern boundary of the study area. Parts of six USGS 7.5' map quadrangles are included. Three types of error are visible. First, there is a quasi-periodic "ripple" of 250- to 300-m wavelength and up to 7-m amplitude, oriented roughly, but not exactly, east-west. Second, there is a quasi-random lumpiness of approximately 20-ha patch size, which varied in amplitude from quadrangle to quadrangle. Third, there are linear discontinuities of up to 15 m in elevation, running north-south and east-west, which often, but not always, agree with quadrangle boundaries. The amplitude of all three types of error varied substantially from quadrangle to quadrangle; the orientation and spatial frequency varies less dramatically. Over water bodies, such as reservoirs, the errors have apparently been removed by the USGS, as they were not present.

The ripple originated from USGS manual profiling of photogrammetric stereo-models (U. S. Geological Survey 1993) and is actually modulated by terrain. Human operators made negative errors (resulting in lower elevations) when scanning in an uphill direction and positive errors when scanning downhill (Band 1993b), so that the phase of the ripple is altered by terrain. This error pattern is therefore difficult to remove using standard de-stripping algorithms such as Fourier filtering (Simpson et al. 1995). If the ripple were a perfect sinusoid superimposed on terrain, it could simply be subtracted from the DEM, but the variable amplitude, wavelength, and phase make this impossible. A disadvantage of the commonly used rectangular box-average method of stripe removal (Brown and Bara 1994) is that it removes real terrain features, such as some east-west trending woody draws in the LMNG (see Chapters 2 and 5 for more detailed discussions of DEM sources and errors). The 7.5' USGS 30-m DEMs are by far the best elevation data available for our study area, so precise quantification and correction of errors, or the side effects of ripple removal methods, cannot be undertaken, because there are no reference data.

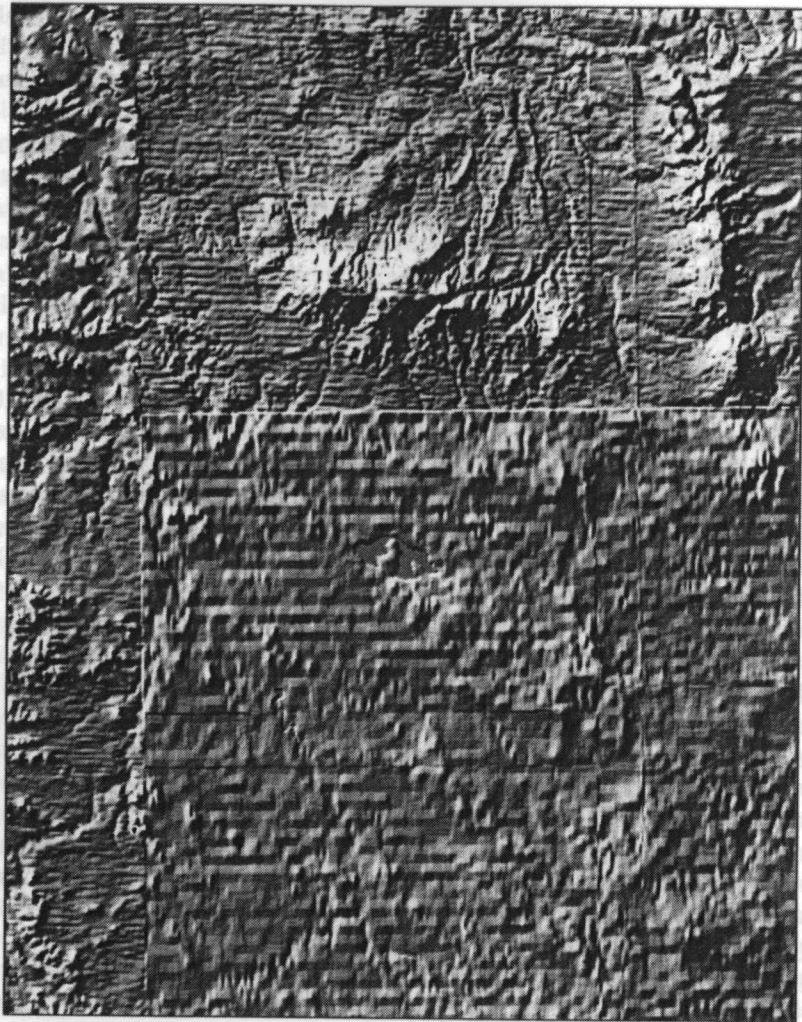


Figure 15.2. Shaded elevation map showing DEM errors in part of study area.

### 15.3.3 Terrain Analysis

The standard suite of primary topographic attributes described in Chapter 3 were calculated with TAPES-G using the following options. First, depressions present in the raw DEM caused by elevation errors such as the ripple pattern and/or the terrain being insufficiently resolved at the 30-m cell size of the DEM were removed. The narrow wooded draws in the LMNG are only a few cells wide, so the bottom of the

channel is not always sampled, producing a chain of "spurious pits" along the drainage path. Second, the FRho8 multiple-flow direction method was used to simulate flow across upland areas with upslope contributing areas of less than 20,000 m<sup>2</sup>. Third, the Rho8 single-flow direction algorithm was used to simulate flow across "channel" cells with upslope contributing areas of 20,000 m<sup>2</sup> or more.

This maximum cross-grading area threshold of 20,000 m<sup>2</sup> was chosen because it provided the best match with the blue stream lines recorded on 7.5' USGS quadrangles. These stream lines were not totally consistent with catchment area since they were derived from photo interpretation. Another approach is to adjust the TAPES-G threshold to give channels that correspond to the pattern of woody draw vegetation seen in the *Landsat* TM image. This yielded a lower catchment area threshold, 10,000 m<sup>2</sup>, because wooded draw vegetation occurred in drainages smaller than those delineated with blue stream lines on topographic maps. One disadvantage of the lower threshold would have been the creation of some spurious channels caused by DEM errors. Typically, these spurious channels trend east-west in the orientation of the "ripple" error, but sometimes north-south quadrangle boundaries produce errors as well (Figure 15.2).

A quasi-dynamic topographic wetness index was calculated with DYNWET (Barling et al. 1994; Chapter 4) and the slope and upslope contributing area outputs from TAPES-G. DYNWET also requires average soil depth, saturated hydraulic conductivity, effective (drainable) porosity, and average drainage time between rainfall events as inputs. A mean soil depth of 0.5 m and a modal soil texture of silt loam were estimated from the Slope County soil survey (Thompson 1978). A saturated hydraulic conductivity of 15 mm/h (Rawls and Brakensiek 1989) and drainable porosity equal to 25% of soil volume (Ratliff et al. 1983) are representative for this soil texture. In reality, soil properties vary across the landscape, but the version of DYNWET implemented for this study assumed that they could be approximated by these spatial averages. A mean drainage time of 10 days was chosen to reflect the typical interval between major precipitation events in the LMNG.

SRAD (Wilson and Gallant 2001; Chapter 4) calculates short-wave (visible) and long-wave (infrared) radiation budgets at each cell in a DEM. For this study, only the incoming short-wave solar radiation was used, because the other components of the radiation budget depend on vegetative cover and to use them in the determination of remote sensing vegetation type would invoke circular reasoning. SRAD uses a three-component approximation of the sky-brightness function. It computes the sum of direct-beam solar radiation, a circumsolar diffuse component scattered from within a few degrees of the solar direction (both affected by topographic shading), and the wider-angle diffuse radiation reflected from blue sky, clouds, and surrounding terrain. To compute this diffuse component, SRAD requires an input parameter,  $\beta$ , that represents the mean transmission coefficient for sunlight passing through clouds. The  $\beta$  parameter was calculated from 1961–1990 mean monthly solar radiation and percent-of-possible-sunshine measured at the nearest station to the LMNG in Bismarck, ND (NOAA 1993b). Incident radiation was computed at four 90-day intervals throughout the year, then added to obtain the mean annual short-wave solar radiation incident on the land surface.

### 15.3.4 Ground-Truth Data

Measurements of dominant overstory vegetation were available from plot data collected by the U. S. Forest Service between 1987 and 1994 at 97 field sites in the five-quadrangle study area. Each site was associated with a vegetation patch visible on the *Landsat* TM image, and each plot was assigned a cover type label from a hierarchical system based on Anderson et al. (1976) (Table 15.1). To increase the sample size for land cover types, such as riparian broadleaf forest, that were poorly represented in the field data, an additional 76 ground-truth sites were obtained from 1:24,000-scale air photos dated 17 August 1981. Some land cover types, such as riparian shrub, sagebrush, and juniper forest, were nevertheless still poorly represented (five plots or less) in the combined data set because they could not be identified on aerial photographs.

### 15.3.5 Performance Evaluation

We took the training data set (173 observations) and removed one plot at a time, using the remaining data to classify each one. If the plot held back was correctly classified by the others, then it was counted along the diagonal of the error matrix; if not, it was counted in the row or column where it was "confused." Steele et al. (1998) have since proposed a new evaluation method based on a true bootstrap process; however, there is very little difference between the error matrices and percent agreements reported here and those that would be obtained with this new method. The accuracy of the overall classification and individual land cover categories were both of interest. In addition, a pixel-by-pixel comparison of the land cover maps can be used to estimate a percent agreement between any pair of maps, indicating how much the addition of topographic attributes or a change in the size of the minimum map unit affects the maps. The percent agreement was computed with the CON function

**TABLE 15.2** Summary Statistics for Topographic Attributes

Topographic Attribute	Study Area				Ground-Truth Sites			
	Min	Max	Mean	SD	Min	Max	Mean	SD
Elevation (m)	695	1024	825	46	731	899	821	40
Slope (%)	0.0	98.9	9.2	8.2	0.0	47.7	10.3	9.2
Upslope contributing area (000 m <sup>2</sup> )	0.9	300	23.7	64.7	0.9	300	57.5	98.8
Steady-state topographic wetness index	4.03	24.50	8.00	2.28	5.02	16.96	8.34	2.13
Quasi-dynamic topographic wetness index	1.64	2.67	2.54	0.17	2.17	2.67	2.53	0.14
Incident short-wave solar radiation (W/m <sup>2</sup> )	77	196	153	10.6	125	185	152	10.5

in ARC/INFO, which can be applied to either the vegetation maps or stream buffers in raster (image) format.

## 15.4 RESULTS

### 15.4.1 Terrain Attribute Maps

Terrain parameters were computed for an area somewhat larger than the five-quadrangle remote sensing area (Figure 15.1) to insure that cumulative hydrologic parameters were complete. The only parts of the TAPES-G upslope contributing area map that do not have complete catchment coverage are the one-cell-wide drainage channels of the Little Missouri River and two of its tributaries. USGS 30-m DEMs were not available for the headwaters of these catchments. However, the channels had very large values of upslope contributing area by the time they entered the study area, and the channels were not resolved in the remote sensing image, so this had a negligible effect on final classification accuracy. The upslope contributing areas computed at the locations of each of the ground-truth sites were based on complete elevation data.

Output grids from TAPES-G, DYNWET, and SRAD are shown in Figures 15.3–15.8. The differences between the gently rolling upland areas at the eastern edge of the study area and the rugged wooded draws and badlands in the western two-thirds of the study area are evident in most of these maps. The abrupt transition between the rolling uplands in the east and the highly dissected Little Missouri drainage to the west is particularly prominent in the slope map (Figure 15.3). Flat areas, shown in dark tones, such as floodplains, river terraces, and depressions in rolling upland, are clearly visible in the slope map (Figure 15.3). They are also visible as areas of large upslope contributing area (Figure 15.4) and as wet areas (light tones) in both the steady-state and quasi-dynamic topographic wetness index maps (Figures 15.5 and 15.6). Ridge lines appear as dark areas (low upslope contributing area) and valleys, floodplains, and depressions appear as light tones (high upslope contributing area) in the upslope contributing area map (Figure 15.4). The distribution of both topographic wetness indices follows a pattern of high wetness in flatter terrain and lower wetness on steeper slopes (Figures 15.3, 15.5, and 15.6).

The upslope contributing area and topographic wetness maps (Figures 15.4–15.6) show numerous spurious linear drainage features trending east–west and confirm that elevation data quality was visibly lower in the northern and eastern USGS quadrangles. Other discontinuities at quadrangle boundaries are visible in the left center part of Figure 15.4, where the flat river terraces and floodplains are truncated by an elevation jump across a quadrangle boundary.

The aspect and short-wave solar radiation maps (Figures 15.7, 15.8) reveal similar patterns; however, topographic shading on north-facing slopes produced a more complex spatial pattern in the short-wave solar radiation map. The white areas in the aspect map show areas with zero slopes for which aspects could not be calculated. In the solar radiation map (Figure 15.8), north-facing slopes receiving 80–100 W/m<sup>2</sup>

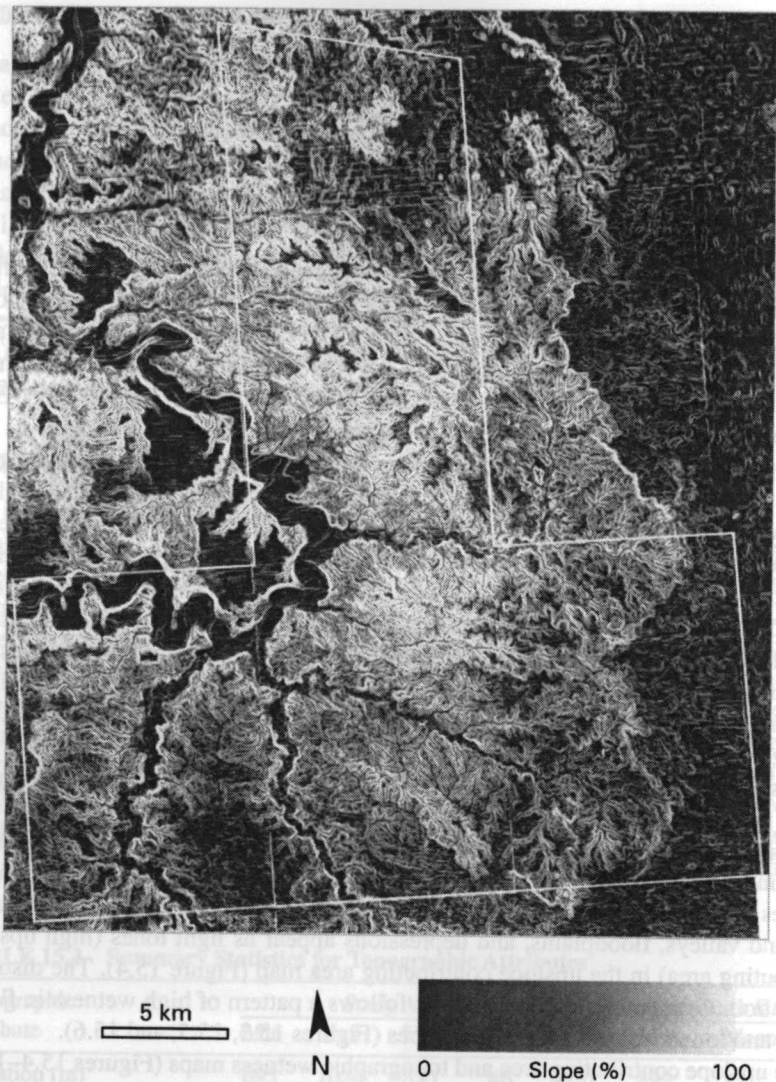
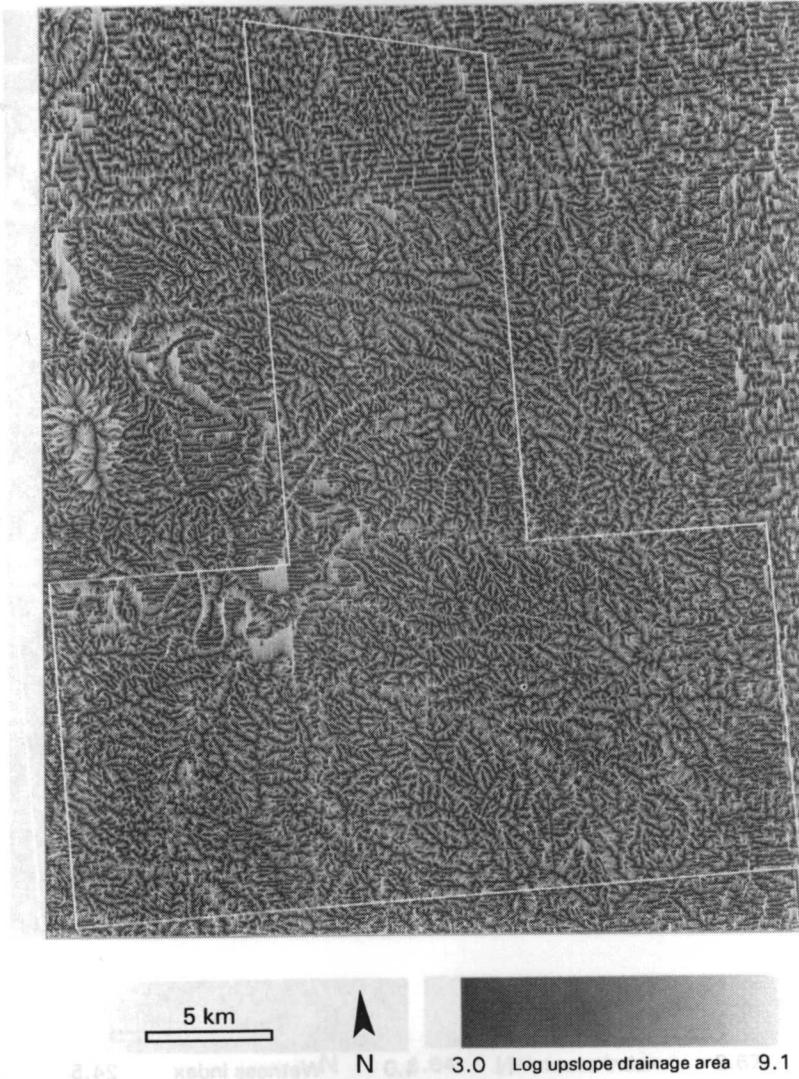


Figure 15.3. Slope map calculated with TAPES-G.

average annual solar radiation are shown in dark tones and southern exposures receiving  $150\text{--}190\text{ W/m}^2$  are shown in lighter tones. More variation in radiation intensity is seen in the badlands (center of map) compared with the gentler rolling terrain to the east. Figure 15.8 also shows a high-frequency ripple in elevation over part of the study area, plus a more pronounced low-frequency ripple in the northern and eastern quadrangles outside the study area.

The magnitude and range of values calculated for each of the topographic attributes mapped in Figures 15.3–15.8 are summarized in Table 15.2. These statistics por-



**Figure 15.4.** Upslope contributing area map calculated with TAPES-G.

tray a relatively flat study area (9.2% average slope, 329 m total relief). Topographic wetness (8.0 mean, 2.3 standard deviation and 2.5 mean, 0.2 standard deviation for steady-state and quasi-dynamic topographic wetness index, respectively) and incident short-wave solar radiation (153 and 11  $\text{W}/\text{m}^2$  mean and standard deviation, respectively) varied little in upland areas (i.e., in those cells not traversed by channels). The corresponding statistics for the 170 ground-truth plots showed that these locations omitted those cells containing the minimum and maximum values reported for most topographic attributes. These sites also exhibited slightly steeper slopes,

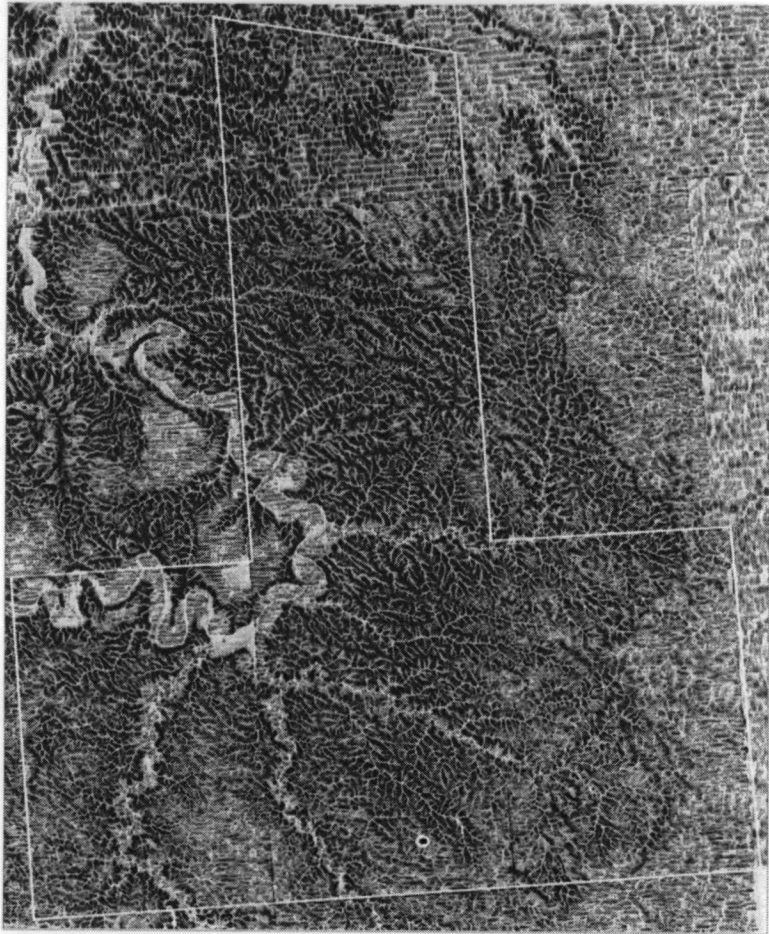


**Figure 15.5.** Steady-state topographic wetness map calculated with DYNWET.

larger upslope contributing areas, and higher steady-state topographic wetness indices compared to the five quadrangle remote sensing study area as a whole.

#### 15.4.2 Land Cover Classification Without Topographic Attributes

The accuracy of the initial land cover classification increased slightly (from 54 to 57%) when the minimum map unit was increased from 0.4 to 0.8 ha and was unaltered when the minimum map unit was increased again to 2.0 ha (Table 15.3). Six

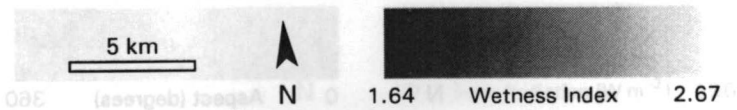
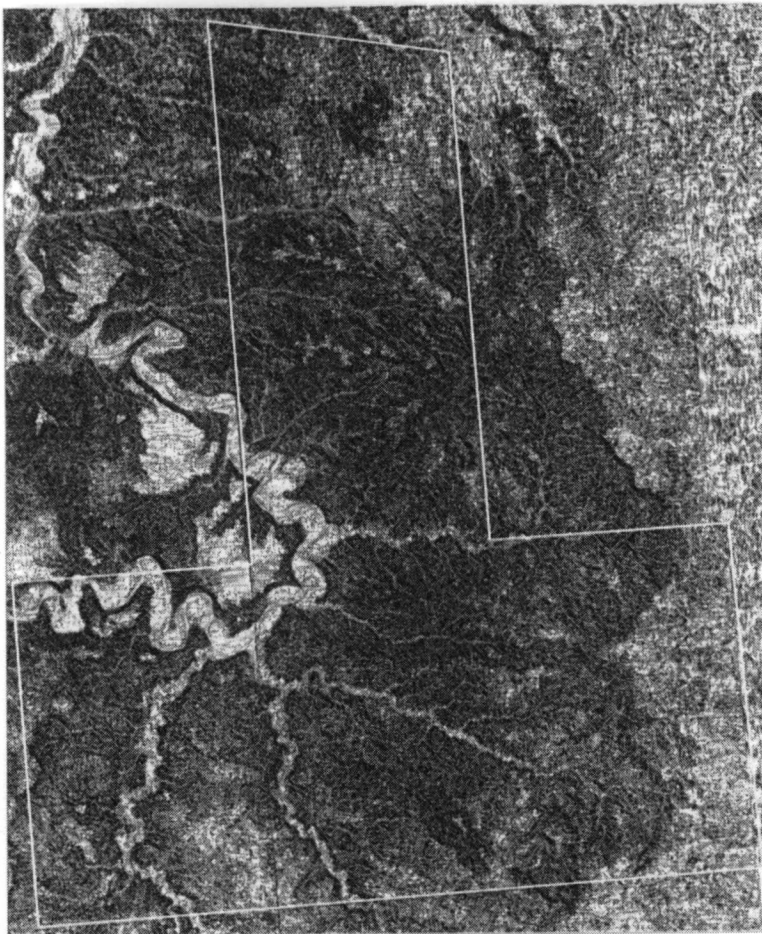


**Figure 15.6.** Quasi-dynamic topographic wetness map calculated with DYNWET.

additional ground-truth sites were correctly classified in each instance. Correct identifications fall along the diagonal in Table 15.3 and incorrect classifications fall elsewhere. Increasing the minimum map unit produced minor changes in the accuracy of individual land cover classifications as follows. First, the number of mesic upland shrub (3201), Rocky Mountain juniper (4214), and riparian grass/forb (6201) sites correctly identified increased as map unit size increased. Second, the number of upland broadleaf forest (4102), water (5000), and badland (7601) sites correctly identified decreased as minimum map unit size increased. Third, the number of crop-

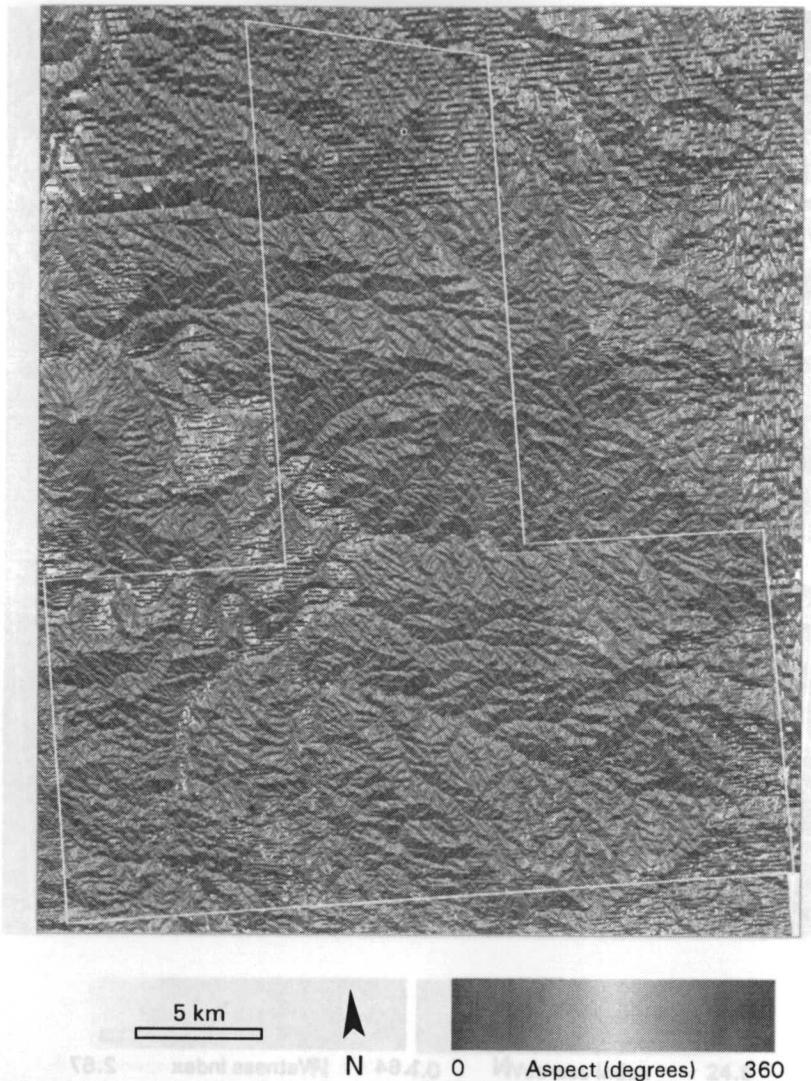


Figure 15.7. Aspect map calculated with TAPES-G.

land (2100), low grass (3110, 3111), and riparian broadleaf forest (6102) sites correctly identified varied as minimum map unit size increased.

However, the number of sites affected was small ( $\pm 3$  sites) for all but two of the classes (mesic upland shrub and riparian broadleaf forest). The errors reveal numerous trends as follows. Several cropland sites were classified as riparian broadleaf forest, shrub, or grass/forb. Numerous low grass/low productivity sites were assigned to the low grass/medium productivity category and vice versa. Several mesic upland shrub sites were classified as riparian broadleaf forest. Upland



**Figure 15.8.** Mean annual short-wave solar radiation map calculated with SRAD.

broadleaf forest was often classified as riparian broadleaf forest. Riparian broadleaf forest was often assigned to the cropland, upland broadleaf forest, or one of the other riparian land cover classes (Table 15.3). Several riparian grass/forb sites were assigned to cropland or one of the other riparian land cover classes. Overall, these results suggest that there may be no disadvantage to using the larger mapping unit in the study area, and this level of aggregation was used to evaluate the results of adding topographic attributes to the final two steps in the classification method as reported below.

**TABLE 15.3 Error Matrices for Land Cover Classifications Prepared With Initial Classification Method and Three Minimum Map Units  
A. 0.4-ha Minimum Map Unit\***

Field Classification	Remotely Sensed Classification											Total		
	2100	3100	3111	3201	3309	4102	4206	4214	5000	6102	6201		6202	7601
2100	12 (67%)				1						2	2	1	18
3110		16 (67%)	8											24
3111		13	7 (33%)	1										21
3201			1	0 (0%)	2	1	2		3	1				10
3309			1	1 (0%)	3 (60%)									5
4102					3	1 (25%)	1		7		1			12
4206				1		7 (88%)								8
4214			1		1		3 (60%)							5
5000								3 (100%)						3
6102					8				24 (60%)	4	4			40
6201	1			2					3	2	1			9
6202	1				1				3		0 (0%)			5
7601													13 (100%)	13
Total	14	29	18	5	5	15	10	3	40	9	8	14	14	173

**B. 0.8-ha Minimum Map Unit<sup>b</sup>**

*Remotely Sensed Classification*

Field Classification	2100	3100	3111	3201	3309	4102	4206	4214	5000	6102	6201	6202	7601	Total
2100	13 (72%)		1		1						1	1	1	18
3110		17 (71%)	6								1			24
3111		11	9 (43%)								1			21
3201				2 (20%)	1	1				5	1			10
3309				1	4 (80%)									5
4102	1					3 (25%)	1			6	1			12
4206					1		7 (88%)							8
4214			1					4 (80%)						5
5000									3 (100%)					3
6102			1	3	1	10				19 (48%)	4	2		40
6201			1							3	4 (44%)	1		9
6202	1									1	1	2 (40%)		5
7601	1												12 (92%)	13
Total	16	28	19	6	7	14	9	4	3	34	14	6	13	173

(continued)

**Table 15.3 (Continued)**  
**C. 2.0-ha Minimum Map Unit \***

Field Classification	Remotely Sensed Classification													Total
	2100	3100	3111	3201	3309	4102	4206	4214	5000	6102	6201	6202	7601	
2100	11 (61%)		1		1					3	1		1	18
3110		15 (63%)	4						1	2			2	24
3111		11	6 (29%)	1						1			2	21
3201		1	1	5 (50%)	1					2				10
3309			1		3 (60%)						1			5
4102				3	2 (17%)				1	5		1		12
4206				1		7 (88%)								8
4214							5 (100%)							5
5000					1	1			1 (33%)					3
6102	3	1	1	1	4					26 (65%)	2	2		40
6201	2									2	5 (56%)			9
6202	1									1	1	2 (40%)		5
7601	1		1										11 (85%)	13
Total	18	28	15	11	3	8	5	3	3	42	10	5	16	173

\*Overall agreement = 54% (numbers in parentheses indicate percent correct in each category).

†Overall agreement = 57%.

\*Overall agreement = 57%.

Note. See Table 15.1 for descriptions of individual land cover classes.

### 15.4.3 Adding Topographic Attributes

Table 15.4 shows the effects of adding quasi-dynamic topographic wetness index and incident short-wave solar radiation to the land cover classification based on a 2.0-ha minimum map unit. Overall and individual class accuracies changed very little ( $\pm 1-3$  sites in each instance), and there was little change in the errors of omission and commission. The explanation for this result is evident in Table 15.5 which shows how all of the topographic attributes except slope exhibited a large amount of overlap between land cover classes. Both secondary topographic attributes, in particular, showed a very large overlap between vegetation classes (Table 15.5). Small ranges in small samples ( $n \leq 5$ ) may simply reflect a lack of data, but a large range in a small sample size does provide evidence of a large variance. Classes 3309 (sagebrush), 4214 (Rocky Mountain juniper forest), and 6202 (riparian shrub) have sample sizes of five or less. The quasi-dynamic topographic wetness indices reached similar maximum values of 2.64–2.67 in all classes except Rocky Mountain juniper forest, and three classes (3110, low grass/low cover; 4102, upland broadleaf forest; 7601, badland) span the entire range of 2.20–2.67 (Table 15.2). Thus, land cover classes were not well separated by this parameter, and this was reflected in the slight reduction in classification accuracy when it was added to the *Landsat* TM data.

In addition, some of the most seriously confused classes, such as 2100 (cropland) and 6102 (riparian broadleaf forest), showed largely overlapping distributions in both quasi-dynamic topographic wetness index and incident short-wave solar radiation (Table 15.5). If steady-state topographic wetness (Figure 15.5) is substituted for quasi-dynamic topographic wetness (Figure 15.6), a similar overlap exists between cropland and riparian broadleaf forest. In the case of incident short-wave solar radiation (Figure 15.8), the riparian forest class has the largest range of values. In contrast, the slope attribute used in the supervised classification process did exhibit interesting variations between land cover classes (Figure 15.3). None of the 18 cropland sites occurred on slopes greater than 10%, whereas 6 of the remaining 11 classes had average slopes  $> 10\%$  and one (4214, Rocky Mountain juniper forest) occurred on slopes exceeding 30%. Thus, slope did show less overlap between some land cover classes than the secondary topographic attributes used in this study (Table 15.5).

### 15.4.4 Use of Stream Buffers to Delineate Riparian and Upland Cover Classes

The topographic attributes calculated with TAPES-G can be used to delineate the channel system, since the channel initiation threshold (drainage density) can be adjusted to delineate additional channels that are not identified in published USGS hydrography DLGs. The maximum cross-grading area specified in TAPES-G to switch from multiple to single flow directions with the *FD8/F8* and *FRho8/Rho8* options was treated as the channel initiation threshold in this study. A maximum cross-grading area of 20,000 m<sup>2</sup> was chosen because it provided the best match with the stream lines recorded on 7.5' USGS quadrangles. These "channel" cells were

TABLE 15.4. Error Matrices for Land Cover Classifications Prepared With Modified Classification Method, 2.0-ha Minimum Map Unit, and One or Two Selected Topographic Inputs  
 A. Landsat TM Bands Plus Elevation, Slope, and Quasi-dynamic Topographic Wetness Index\*

Classification Field	Remotely Sensed Classification													Total
	2100	3100	3111	3201	3309	4102	4206	4214	5000	6102	6201	6202	7601	
2100	10 (56%)		1							4	1	1	1	18
3110		16 (67%)	4		1				1	1			1	24
3111		12	5 (24%)	1						1			2	21
3201			2	5 (50%)		1				2				10
3309			1		3 (60%)						1			5
4102				2		4 (33%)			1	5				12
4206							7 (88%)			1				8
4214								5 (100%)						5
5000						1	1		1 (33%)					3
6102	4	1	1	2	5					25 (63%)		2		40
6201	2	6								2	5 (56%)			9
6202	1									1	1	2 (40%)		5
7601	1		1										11 (85%)	13
Total	18	29	15	10	4	11	8	5	3	42	8	5	15	173

**D. LANDSAT 1 IN DATA PLUS ELEVATION, SLOPE, QUASI-DYNAMIC TOPOGRAPHIC WETNESS INDEX, AND INCIDENT SHORT-WAVE SOLAR RADIATION\***

*Remotely Sensed Classification*

Field Classification	2100	3100	3111	3201	3309	4102	4206	4214	5000	6102	6201	6202	7601	Total
2100	10 (56%)		1		1					3	2		1	18
3110		17 (71%)	4	1					1	1				24
3111		11	6 (29%)	1						1			2	21
3201		2	1	4 (40%)	1	1				1	1			10
3309				1 (40%)	3 (60%)				1	1				5
4102	1			2		2 (17%)			1	5		1		12
4206							7 (88%)				1			8
4214						2	1	2 (40%)						5
5000				1	1				1 (33%)					3
6102	3	1	1	2		4				26 (26%)	1	2		40
6201	1									2	5 (56%)			9
6202	1						1				1	3 (60%)		5
7601	1		1										11 (85%)	13
Total	17	31	14	11	5	10	9	2	3	40	11	6	14	173

\*Overall agreement = 57%.

<sup>b</sup>Overall agreement = 56%.

Note: See Table 15.1 for definitions of individual land cover classes.

TABLE 15.5 Topographic Attribute Summary Statistics by Land Cover Type

Variable	Min	Max	Mean	SD	Min	Max	Mean	SD	Min	Max	Mean	SD
<b>Cropland (n = 18)</b>												
Elev (m)	734	882	807	48	778	899	846	35	778	889	834	41
Slope (%)	1.7	9.1	4.6	2.6	0.7	35.5	7.1	7.0	0.1	20.8	7.0	5.6
Aspect (deg.)	0	315	122	109	0	315	144	104	0	346	138	108
Upslope (000 m <sup>2</sup> )	0.90	204.2	32.4	57.2	0.90	190.5	15.7	39.4	0.90	300.0	20.3	64.6
SS TWI	6.92	11.46	8.48	1.43	5.45	11.22	7.70	1.31	5.93	13.12	8.09	1.70
QD TWI	2.34	2.67	2.59	0.11	2.21	2.67	2.46	0.14	2.32	2.67	2.54	0.11
Solar (W/m <sup>2</sup> )	128	165	153	8.4	139	180	155	10.3	135	172	150	9.1
<b>Riparian grass/forb (n = 9)</b>												
Elev (m)	806	860	840	20	773	829	798	20	750	807	775	21
Slope (%)	1.3	19.4	5.5	5.7	2.1	29.5	11.3	8.2	0	19.2	5.6	7.8
Aspect (deg.)	0	342	131	122	0	281	138	112	0	270	176	113
Upslope (000 m <sup>2</sup> )	1.7	300.0	167.9	156.7	0.9	300.0	79.8	118.0	11.8	300.0	166.8	131.3
SS TWI	5.83	14.46	10.39	3.01	5.78	12.32	8.70	2.08	6.51	14.37	9.52	2.94
QD TWI	2.48	2.67	2.60	0.07	2.37	2.66	2.57	0.10	2.63	2.67	2.66	0.02
Solar (W/m <sup>2</sup> )	140	168	154	8.2	136	160	149	7.9	153	165	157	5.5
<b>Sagebrush (n = 5)</b>												
Elev (m)	741	780	768	16	787	886	833	31	785	872	835	29
Slope (%)	0.3	7.1	3.6	2.9	2.1	42.7	19.7	14.6	4.8	35.1	18.5	7.7
Aspect (deg.)	0	236	158	91	0	227	119	86	11	315	149	121
Upslope (000 m <sup>2</sup> )	0.9	300.0	141.0	147.0	0.9	7.8	2.0	1.8	6.6	300.0	69.5	100.0
SS TWI	7.29	14.02	11.53	2.81	5.08	8.82	6.25	1.19	6.61	14.11	8.48	2.11
QD TWI	2.64	2.67	2.66	0.01	2.21	2.67	2.41	0.18	2.20	2.64	2.45	0.14
Solar (W/m <sup>2</sup> )	132	153	141	8.3	142	163	155	6.2	134	164	152	9.7
<b>Riparian broadleaf forest (n = 40)</b>												
Elev (m)	731	878	813	41	778	810	797	10	833	872	846	16
Slope (%)	1.1	25.8	10.3	5.3	5.6	16.5	11.0	3.8	20.1	47.7	34.2	11.5
Aspect (deg.)	0	333	191	91	7	349	156	151	274	350	309	32
Upslope (000 m <sup>2</sup> )	1.8	300.0	90.4	110.3	0.9	4.9	2.6	1.5	1.7	17.4	8.9	7.0
SS TWI	5.53	16.96	8.89	2.07	6.1	7.5	6.7	0.48	5.02	7.69	6.47	1.28
QD TWI	2.34	2.67	2.56	0.11	2.33	2.65	2.54	0.12	2.17	2.54	2.34	0.16
Solar (W/m <sup>2</sup> )	130	185	154	11.9	129	168	148	15.1	125	164	144	18.4
<b>Ponderosa pine forest (n = 8)</b>												
<b>Badlands (n = 13)</b>												
<b>Mesic upland shrub (n = 10)</b>												
<b>Riparian shrub (n = 5)</b>												
<b>Upland broadleaf forest (n = 12)</b>												
<b>Rocky Mountain Juniper (n = 5)</b>												

used with the 5-m elevation threshold to delineate riparian and upland areas. This method designated 16.0% (272 km<sup>2</sup>) of the study area as riparian (Figure 15.9) compared to only 11.4% (194 km<sup>2</sup>) using the 0.5° by 1° USGS hydrography DLGs (Figure 15.10). The DEM errors reported earlier produced some spurious drainages trending east–west in low-relief areas (see east side of Figure 15.9). About 117 km<sup>2</sup> was designated as riparian by both methods notwithstanding these problems. Agreement was generally good in the middle sections of well-defined, wooded draws, but worse in source areas and in flatter rolling upland terrain (cf. Figures 15.3, 15.9, and 15.10). However, the choice of 5 m as the elevation threshold may have overestimated riparian areas in both instances because this threshold produced very wide buffers ( $\leq 0.5$  km) in areas of low relief, such as river terraces and rolling upland (cf. Figures 15.9 and 15.10).

The computed riparian zones did not match the satellite-based land cover classification very well. For example, only 39% of the 365 km<sup>2</sup> assigned to riparian land cover classes with the initial classification method (2.0-ha minimum map unit) was located in the riparian areas delineated with the TAPES-G stream network and the 5-m elevation threshold. Similarly, 47.5% of the TAPES-G riparian area was assigned to nonriparian land cover classes with the initial classification method, and these areas should be removed from the modeled riparian zone. We had hoped to be able to use the riparian zones to separate out riparian and upland land cover classes with similar spectral signatures. However, the five upland broadleaf forest training sites classified as riparian broadleaf forest and four riparian broadleaf forest training sites classified as upland broadleaf forest with the initial land cover classification (2.0-ha minimum map unit; Table 15.3C) were not resolved when the USGS and TAPES-G stream buffers were applied. Overall, these results indicate that different methods and data sources will delineate very different riparian zones and these may not help with the correct identification of cover classes that have similar spectral signatures but grow in different landscape positions. Hence, the riparian zones computed with this step were not used to revise the land cover maps discussed in the next section.

#### 15.4.5 Evaluation of Land Cover Maps

Land cover maps for a representative area in the southeast part of the study area are reproduced in Figure 15.11 (see color insert). Some confusion between cropland and riparian forest remains in all cases: For example, the rectangular cultivated field in the lower left corner of the maps is erroneously classified as ponderosa pine or riparian forest, even when topographic attributes are added to the classification. Changing the spatial aggregation from 0.4 to 0.8 ha and then 2.0 ha altered some map unit identifications, but many misclassifications still remained.

Although overall classification accuracy varied little between different levels of spatial aggregation and topographic attribute combinations, a pixel-by-pixel comparison of the vegetation maps shows substantial differences between them. Percent agreement between the 36 unique combinations of minimum map unit and classification method is summarized in Table 15.6. The addition of topographic attributes holding minimum map unit size constant generated 67–89% agreement, which

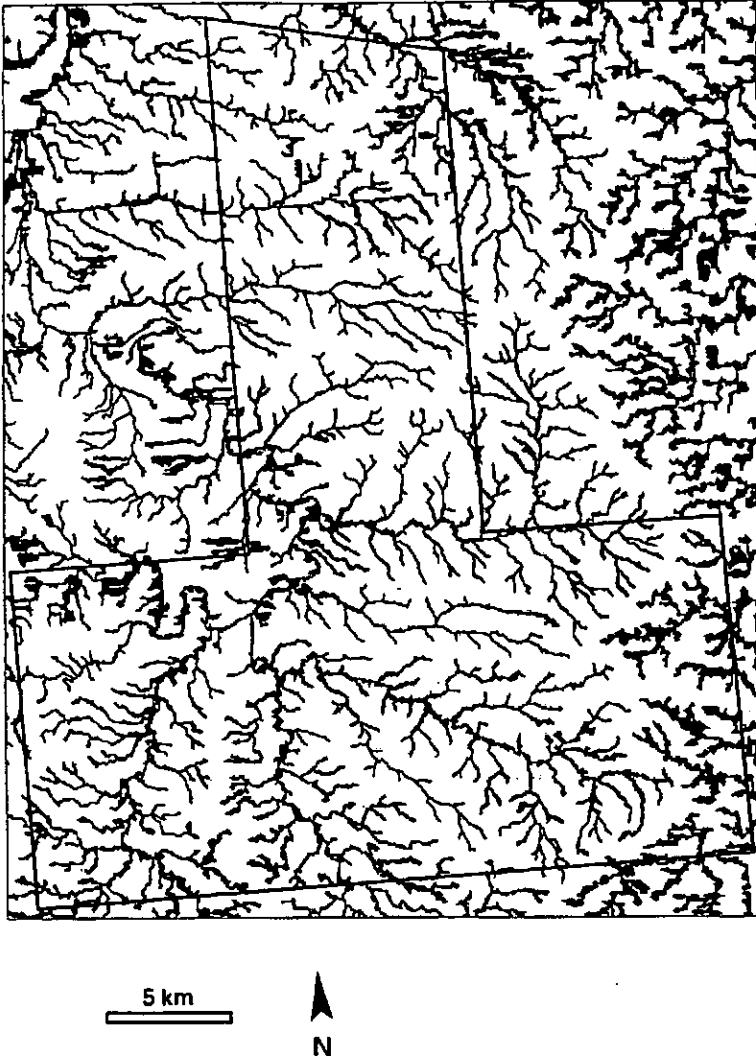


Figure 15.9. Stream elevation buffer computed from TAPES-G stream network.

means that up to 33% of the pixels in the map were reclassified with the addition of one or two secondary topographic attributes. Figures 15.11A–C show how the classification changes with the addition of topographic attributes for the 0.4-ha mapping unit. Varying the minimum map unit produced even lower agreement, only 34–44%; in other words, between 56 and 66% of the pixels were reclassified when the level of spatial aggregation was varied from 0.4 to 2.0 ha. This is evident in Figures 15.11A, D, and E, where the spatial pattern of vegetation patches varies greatly, depending on the level of spatial aggregation. Ultimately, the choice of minimum map unit is a mat-



Figure 15.10. Stream elevation buffer computed from USGS hydrography DLGs.

ter of user preference, but since the aggregation process cannot be reversed, it may be advisable to underestimate the size of mapping unit, to preserve ecologically valuable information in small vegetation patches.

Although there is no loss of overall accuracy in a 2.0-ha aggregation, the spatial pattern of wooded draw vegetation in the LMNG is more difficult to discern in the aggregated image. For example, the narrow strips of riparian broadleaf forest (class 6102), shown in magenta in the bottom part of Figure 15.11C, are visible with a 0.4-ha minimum map unit, but are replaced with three large patches when the 2.0-ha min-

**TABLE 15.6 Percent Agreement Based on Pixel-by-Pixel Comparison of Land Cover Maps**

Classification	L0.4	L0.8	L2.0	W0.4	W0.8	W2.0	S0.4	S0.8	S2.0
<i>Landsat</i> <sup>a</sup> (0.4 ha)	—								
<i>Landsat</i> <sup>a</sup> (0.8 ha)	41.7	—							
<i>Landsat</i> <sup>a</sup> (2.0 ha)	43.2	36.8	—						
Wetness <sup>b</sup> (0.4 ha)	84.8	41.2	43.1	—					
Wetness <sup>b</sup> (0.8 ha)	41.8	87.5	36.8	42.8	—				
Wetness <sup>b</sup> (2.0 ha)	43.2	36.4	89.4	43.8	37.5	—			
Solar <sup>c</sup> (0.4 ha)	67.1	39.9	40.9	69.8	40.5	41.7	—		
Solar <sup>c</sup> (0.8 ha)	39.9	70.3	35.6	39.2	73.8	35.9	41.3	—	
Solar <sup>c</sup> (2.0 ha)	40.9	34.4	69.6	41.7	35.9	71.6	42.0	39.0	—

<sup>a</sup>Initial (unmodified) classification method.

<sup>b</sup>Modified classification method plus quasi-dynamic topographic wetness index and specified minimum map unit.

<sup>c</sup>Modified classification method plus quasi-dynamic topographic wetness index, short-wave solar radiation, and specified minimum map unit.

imum map unit is used (Figure 15.11E). These large riparian broadleaf forest patches were classified as either upland broadleaf forest (class 4102), Rocky Mountain juniper forest (class 4214), riparian grass and forb (class 6201), or riparian shrub (class 6202) in the three classifications produced using a 0.4-ha minimum map unit (cf. Figures 15.11A–C, E).

## 15.5 DISCUSSION

The overall results produced in this study (~55% classification accuracy using 12 land cover classes plus water) matches that achieved in other remote sensing classifications of land cover. Higher levels of accuracy can be achieved by merging vegetation classes with similar spectral signatures. Table 15.7 shows how a reduction of the number of land cover classes from 12 to 7 increased overall classification accuracy to approximately 70% in this instance. However, this strategy is helpful only where land managers do not want or need to delineate large numbers of land cover classes.

We added two additional topographic attributes to our classification method in hopes of improving accuracy without reducing the number of land cover classes. We were clearly unsuccessful and the negligible improvement in classification accuracy gained by adding quasi-dynamic topographic wetness index, incident solar radiation, and riparian buffers to distinguish upland and riparian vegetation classes would not seem to justify the use of topographic attributes in remote sensing vegetation mapping. Six sets of issues should be investigated further before applying terrain analysis to a large geographic area such as the LMNG:

- Utilization of additional ground-truth data and/or satellite imagery
- Inclusion of topographic attributes in the first stage of the classification method used here

**TABLE 15.7 Error Matrices for Generalized Land Cover Classifications Prepared With Modified Classification Method and One or More Selected Topographic Attributes**  
**A. Landsat TM Bands Plus Elevation and Slope (2.0-ha minimum map unit)<sup>a</sup>**

Field Classification	Remotely Sensed Classification							Total
	2100	3110 3111 6201	3201 6202	3309 7601	4102 6102	4206 4214	5000	
2100	11 (61%)	2		1	4			18
3110, 3111, 6201	2	41 (76%)	1	4	5		1	54
3201, 6202	1	3	7 (47%)		4			15
3309, 7601	1	3		14 (78%)				18
4102, 6102	3	4	7		37 (71%)		1	52
4206, 4214			1			12 (92%)		13
5000					1	1	1 (33%)	3
Total	18	53	16	19	51	13	3	173

**B. Landsat TM Bands Plus Elevation, Slope, and Quasi-dynamic Topographic Wetness Index (2.0-ha minimum map unit)<sup>b</sup>**

Field Classification	Remotely Sensed Classification							Total
	2100	3110 3111 6201	3201 6202	3309 7601	4102 6102	4206 4214	5000	
2100	10 (56%)	2	1	1	4			18
3110, 3111, 6201	2	42 (78%)	1	4	4		1	54
3201, 6202	1	3	7 (47%)		4			15
3309, 7601	1	3		14 (78%)				18
4102, 6102	4	2	6		39 (75%)		1	52
4206, 4214					1	12 (92%)		13
5000					1	1	1 (33%)	3
Total	18	52	15	19	53	13	3	173

(continued)

Table 15.7 (Continued)

C. Landsat TM Bands Plus Elevation, Slope, Quasi-dynamic Topographic Wetness Index, and Incident Short-Wave Solar Radiation (2.0-ha minimum map unit)<sup>c</sup>

Field Classification	Remotely Sensed Classification							Total
	2100	3110 3111 6201	3201 6202	3309 7601	4102 6102	4206 4214	5000	
2100	10 (56%)	3		1	4			18
3110, 3111, 6201	1	43 (80%)	1	3	4	1	1	54
3201, 6202	1	5	7 (47%)		2			15
3309, 7601	1	1	1	14 (78%)	1			18
4102, 6102	4	3	7		37 (74%)		1	52
4206, 4214		1			2	10 (77%)		13
5000			1	1			1	3 (33%)
Total	17	56	17	19	50	11	3	173

<sup>a</sup>Overall agreement = 71%.

<sup>b</sup>Overall agreement = 72%.

<sup>c</sup>Overall agreement = 71%.

Note. See Table 15.1 for descriptions of individual land cover classes.

- Quantification of the DEM error over the entire Little Missouri region and how it is propagated with computed topographic attributes
- Exploration of the viability and impact of using a more sophisticated topographic wetness index that incorporates the effects of spatially variable precipitation and evapotranspiration
- Inclusion of a more sophisticated buffer algorithm in which the elevation threshold is a function of local vertical relief and/or upslope drainage area, and validation of the stream elevation buffer results with ground-truth data
- Inclusion of additional ancillary data layers in the classification

The bootstrap results used to assess classification accuracy in this chapter were originally generated to identify weaknesses in the training data set. The large omission and commission errors in Tables 15.3 and 15.4 suggest that a larger training set may have helped. Similarly, multitemporal analysis of Landsat TM or AVHRR imagery throughout the growing season might have helped to resolve some of the confusion between the vegetation classes. Cropland, for example, is likely to exhibit rapid changes in spectral signature due to plowing and harvest, compared with the more

constant signature of broadleaf forest in the summer months. Time-series remote sensing has improved accuracy in other large-scale mapping projects (e.g., Pickup et al. 1993, Samson 1993, Fuller et al. 1994). However, in the Konza Prairie, KS, a grassland site similar to the LMNG, Oleson et al. (1995) found that cropland and forest had considerable overlap in spectral signature at all times during the May to October growing season. Both of these options—collecting more ground-truth data and using multitemporal satellite imagery—were prohibited due to limited project funds.

Some improvement might have been gained by modifying the classification method to accommodate multidimensional combinations of the *Landsat* TM bands and selected band transforms as well as the original TM bands. In one such study, Lauer and Whistler (1993) utilized *Landsat* TM2, TM4, TM5, TM7, and NDVI to identify 77 previously unknown natural grassland areas in Anderson County, KS. The six 30-m TM bands plus NDVI and the TM tasseled cap features of brightness, greenness, and wetness (Crist and Cicone 1984) were examined in this study, and the results demonstrated that their final methodology was faster and more accurate than aerial photographs and aerial surveys. Similarly, Anderson et al. (1993) utilized a single *Landsat* TM scene and showed that it is possible to relate vegetation indices to green biomass measurements when data are combined in greenness strata for a semi-arid rangeland study area in northeastern Colorado.

...The methodology of Lauer and Whistler (1993) is instructive for the current study because they performed a multistage classification and filtered the output map to produce a final map of potential high-quality grasslands of 2 ha or larger. We averaged topographic attributes before the supervised classification was performed. Ma and Redmond (1996, personal communication) observed a loss of continuity in riparian corridors at the 2.0-ha aggregation in other parts of the LMNG. The incorporation of topographic attributes in the initial classification step may have improved classification accuracy in this study. At large minimum map units, the computed topographic attributes are averaged over a large area and this may diminish their impact on the classification process. Dividing the initial classification into classes based on topographic attributes will identify landscape units identified in traditional maps (see descriptions in Table 15.1 for examples) and may therefore improve classification accuracy. Dikau (1989) has proposed a landscape classification scheme that divides catchments (hillslopes) into 16 landform classes based on plan and profile curvature, two of the attributes computed with TAPES-G. Burrough et al. (2000a, b), in contrast, have proposed an automated method of landscape classification that incorporates spatial sampling methods, statistical modeling of the derived stream topology, and fuzzy *k*-means using the diagonal metric. Either approach might have generated better predictions, especially if steps were taken to measure and/or eliminate DEM errors.

USGS DEM error varies greatly from quadrangle to quadrangle, and may produce unacceptable errors in topographic attributes in the rolling upland areas of the Little Missouri Grassland. The root mean square error (RMSE) of 7 m that is often reported for 7.5' USGS quadrangles provides a global measure of vertical accuracy that is of little value in assessing the question of topographic attribute uncertainty (Kumler 1994, Hunter et al. 1995, Hunter and Goodchild 1996). Small errors in the horizontal positions and/or elevations of landforms represented in DEMs may lead to large

errors in computed primary and secondary topographic attributes (e.g., Wilson et al. 1998). In the LMNG, the 7.5' USGS elevation data are by far the best available: Quantification of errors is hampered by the lack of a reference data set of accurate elevations with which to compare USGS data. Florinsky (1998) has proposed a series of measures of root mean square errors for slope, aspect, plan, and profile curvature that can be mapped and used to depict the spatial distribution of errors within study sites. Burrough et al. (2000a, b) have suggested adding random errors to DEMs, calculating selected attributes multiple times, and calculating cell averages to minimize these errors. Visual inspection of topographic attribute maps can, of course, provide an excellent qualitative impression of whether the linear patterns of DEM error obliterate terrain features.

A more sophisticated topographic wetness index that incorporates the combined effects of spatially variable precipitation and evapotranspiration might be more successful in discerning vegetation types as well (e.g., Moore et al. 1993e). The level 3 analysis incorporated in WET uses spatially variable net radiation to compute potential evapotranspiration at each grid cell and then determines soil-water content using a set of functional relationships based on soil-water content, evapotranspiration, and deep drainage (see Chapter 4 for additional details). Both evapotranspiration and deep drainage are dependent on soil-water content using this approach. Similarly, the TAPES-G derived buffer should be compared and calibrated, if possible, with ground-truth data such as field maps or air photos showing riparian areas before proceeding with a stream buffer calculation over a larger area.

Bendix (1994) examined the role of scale-specific environmental factors in shaping the pattern of riparian vegetation for two mountainous streams in southern California. Three transverse-scale (distance above water table, flood severity, substrate texture) and five longitudinal-scale variables (elevation, valley orientation, valley width, fire history, lithology) were examined. The regression results showed that the transverse and longitudinal variables jointly influenced the vegetation patterns and observed patterns along different reaches reflect a subtle combination of overlapping gradients. These results may be site-specific and the contribution of longitudinal variables might be reduced in flatter landscapes such as the LMNG.

This study suggests that local (i.e., site-specific) scale thresholds may be required to guide the choice of the channel initiation threshold in TAPES-G and the height that riparian zones extend above stream level. The channel initiation threshold determines the density of drainage channels and the height threshold determines the width of the buffers. Adjusting these values to match the observed riparian vegetation may result in a more useful stream buffer. The calculated stream buffers reproduced in Figures 15.9 and 15.10 suggest that a single height above stream level for the entire area may not be able to generate suitable buffers in both rolling upland and wooded draw areas. The buffer height might be estimated as a function of local vertical relief, so that the height is increased in areas of large vertical relief and reduced in areas of low relief. Alternatively, the roughness (vertical relief divided by area) of each catchment could be computed and used to adjust the buffer threshold used with individual streams. Finally, the threshold could also be scaled by upslope drainage area within each of

the catchments if longitudinal-scale variables were thought to exert a large impact on riparian vegetation patterns.

A combination of one or more of these improvements to the terrain analysis methods may improve results. Additional data layers, such as soil properties and property ownership, might be of some use in improving performance as well. Moore et al. (1993b) have demonstrated a strong correlation between soil properties and computed topographic attributes, so soil mapping may not add much new information. In addition, soils have not been mapped in county soil surveys at sufficient spatial resolution to distinguish the small wooded draws that affect vegetation patterns in the Little Missouri Grassland (Thompson 1978). In other areas, where geologic parent material is more diverse than in the LMNG, soil mapping might improve classification accuracy when incorporated into the classification. Property ownership maps might be of use in identifying cropland, which occurs almost exclusively on private land, although riparian areas also occur on private land. These riparian areas meander through the complex checkerboard pattern of land ownership in the LMNG, making identification by property ownership difficult. This state of affairs illustrates how disturbance and succession are intertwined in the processes that produce spatial patterns of vegetation in these types of landscapes.

## 15.6 CONCLUSIONS

The negligible improvement in classification accuracy gained by the use of a quasi-dynamic topographic wetness index and average incoming short-wave solar radiation does not appear to justify the considerable effort involved in calculating these topographic attributes. From this analysis, it appears that the addition of secondary topographic attributes to remote sensing classifications of semiarid grasslands provides no significant increase in accuracy. It was hoped that distinctions between similar spectral types, such as riparian and upland broadleaf forest in the LMNG, could be made with terrain analysis, but this hypothesis is not supported by this study. East of the Little Missouri, in areas with less vertical relief, such as the Grand River, Cedar River, and Sheyenne National Grasslands, topographic attributes may be of even less use, since the DEM errors are large compared to the vertical relief. The low relief and sparse vegetation cover of the LMNG suggest that additional ground-truth data and multitemporal satellite imagery were required. Both of these options were prohibited due to limited project funds. The inclusion of topographic attributes in the supervised classification, quantification of DEM error over the entire Little Missouri region, and inclusion of additional ancillary data layers may have helped to offset these shortcomings. The results of the current study do demonstrate (1) the benefits of using modern terrain analysis tools to identify channel systems, and (2) that the final land cover maps must be used with care because different source data and levels of spatial aggregation will predict different patterns of existing vegetation.